

## Hygro-thermal post-buckling analysis of a functionally graded beam

Şeref D. Akbaş\*

*Department of Civil Engineering, Bursa Technical University,  
Yıldırım Campus, Yıldırım, Bursa 16330, Turkey*

*(Received May 10, 2019, Revised October 22, 2019, Accepted October 23, 2019)*

**Abstract.** This paper presents post-buckling analysis of a functionally graded beam under hygro-thermal effect. The material properties of the beam change through height axis with a power-law function. In the nonlinear kinematics of the post-buckling problem, the total Lagrangian approach is used. In the solution of the problem, the finite element method is used within plane solid continua. In the nonlinear solution, the Newton-Raphson method is used with incremental displacements. Comparison studies are performed. In the numerical results, the effects of the material distribution, the geometry parameters, the temperature and the moisture changes on the post-buckling responses of the functionally graded beam are presented and discussed.

**Keywords:** functionally graded beam; hygro-thermal effect; post-buckling analysis; total Lagrangian; finite element method

### 1. Introduction

Hygro-thermal effects, namely moisture changes are very important role in the mechanics of the structural elements. Especially, nuclear power plants, aerospace vehicles, thermal power plants etc. are subject to large hygro-thermal loadings. After a certain moisture value, the structural elements can be lost their strength. Functionally graded materials (FGMs) are a type of composite which properties of materials change in a direction. Generally, FGMs are used the thermal barrier systems which produced metal and ceramic materials. As compared to the conventional composite materials, FGMs perform more fracture-resistance and structural strength. With the development of technology, FGMs are used in many engineering projects such as aircrafts, space vehicles, power plants. In FGM structural elements with immovable ends, the buckling and post-buckling cases occurs with temperature or moisture effects. So, understanding the hygro-thermal effects on the FGM structures is very important.

In the literature, a lot of investigations have been given to thermal analysis of FGM beams. However, hygro-thermal studies about FGM structures are not investigated broadly. In recent years, some studies of hygro-thermal effect in the FGM structural elements are published in the literature; Zenkour (2013) investigated the hygrothermal analysis of exponentially graded

---

\*Corresponding author, Ph.D., E-mail: [serefda@yahoo.com](mailto:serefda@yahoo.com)

rectangular plates. Akbarzadeh *et al.* (2013) analyzed hygrothermal responses of a functionally graded piezoelectric media. Kocatürk and Akbaş (2011, 2012), Akbaş and Kocatürk (2012, 2013) investigated post-buckling behavior homogeneous and non-homogeneous beams under temperature effects. Laoufi *et al.* (2016) analyzed the effects of the moisture on the deflection and stress responses of the FGM plates resting on elastic foundation. Beldjelili *et al.* (2016) presented hygrothermal analysis of functionally graded plates embaded on elastic foundation. Mohammadimehr *et al.* (2016) examined static, dynamic and stability of microplate reinforced functionally graded carbon nanotubes under hygro-thermo-mechanical environment. Akbaş (2014, 2015, 2017a, 2017b, 2018a, 2018b, 2018c, 2019) analyzed post-buckling responses of functionally graded and laminated beams under thermal and mechanical loads by using finite element method. Barati (2017) studied dynamic analysis of nano porous FGM plates under hygro-thermal effects. Mouffoki *et al.* (2017) investigated vibration analysis of nanobeams under hygro-thermal effects by using a higher order beam theory. Ebrahimi and Habibi (2018) presented nonlinear behavior of a polymer-carbon nanotube-fiber multiscale nanocomposite plate under hygro-thermal load by using finite element method based on von Kármán geometrical nonlinearity. Jouneghani *et al.* (2018) investigated the hygro-thermal effects of FGM nano structures. Kaci *et al.* (2018) used the a higher order beam theory for post-buckling responses of composite beams. Nguyen *et al.* (2017) analyzed dynamic and stability of FGM beams under moisture effects by using the Ritz method. Lee and Kim (2013) investigated nonlinear hygro-thermal effects of FGM structures. Radwan (2017) examined non-linear hygrothermal effects of FGM sandwich plates resting on elastic foundation. Karami *et al.* (2018) examined wave dispersion of FGM nanoplates by using quasi-3D plate theory under hygro-thermal effect. Abazid *et al.* (2018) analyzed hygrothermal bending of FGM sandwich plates resting on Pasternak foundation.

As seen from the literature, post-buckling and nonlinear studies of FGM structures under hygro-thermal loading have not been investigated in detail. The novelty in this work consists on the post buckling behavior of a FGM beam under hygro-thermal. In the modeling and solution of the problem, the finite element method is implemented with Total Lagrangian two dimensional solid continua. Another novelty of this study is using two dimensional solid continua model which gives more realistic results in contrast with the beam theories such as Euler-Bernoulli, Timoshenko and higher order beam theories. In nonlinear solution, Newton-Raphson is used with incremental displacement. Effects of the material parameter and the hygro-thermal loading on post-buckling deflections of FGM beam are investigated. Also, comparison studies are presented.

## 2. Theory and formulation

A FGM pinned-pinned beam with height  $h$ , length  $L$ , width  $b$  under non-uniform temperature and moisture rising is shown in Fig. 1. Temperature rising of bottom surface indicates as  $\Delta T_B$ , whereas temperature rising of top surface indicates as  $\Delta T_T$ . Moisture content of the bottom surface indicates as  $C_B$ , whereas moisture content of the top surface indicates as  $C_T$ . As seen from figure 1, because the boundary conditions have immovable ends, the buckling or post-buckling cases occur with increasing temperature rising.

The material properties ( $P$ ) change though height axis based on following power-law function distribution

$$P(Y) = (P_T - P_B) \left( \frac{Y}{h} + \frac{1}{2} \right)^n + P_B \quad (1)$$

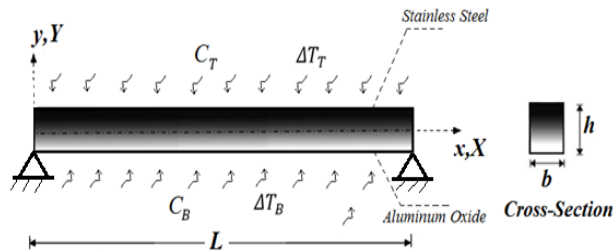


Fig. 1 A pinned-pinned FGM beam under non-uniform moisture and temperature rising

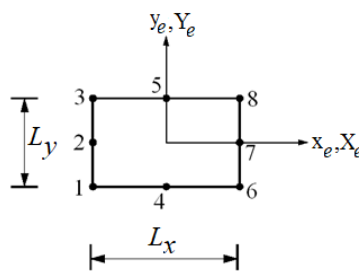


Fig. 2 Eight -node plane element

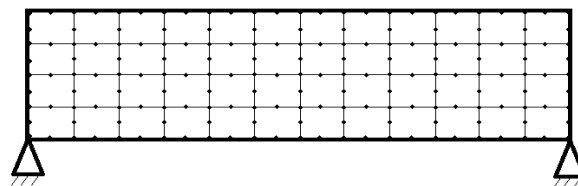


Fig. 3 Finite element model of the problem

where  $P_B$  and  $P_T$  are material properties of bottom and top surfaces,  $n$  is the power-law coefficient (material distribution parameter). According to equation (1), when  $Y=-h/2$ ,  $P=P_B$ , and when  $Y=h/2$ ,  $P=P_T$ . when  $n=0$  material of beam gets homogenous full top material, and when  $n=\infty$  material of beam gets homogenous full bottom material. The temperature rise  $\Delta T = \Delta T(Y)$  is obtained with using heat transfer formulation

$$-\frac{d}{dY} \left[ k(Y) \frac{d\Delta T(Y)}{dY} \right] = 0 \tag{2}$$

where  $k$  indicates the coefficient of thermal conductivity. After integration the equation (2), the following expression can be obtained

$$T(Y) = \Delta T_B (\Delta T_T - \Delta T_B) \int_{-0.5h}^y \frac{1}{k(Y)} dY \Big/ \int_{-0.5h}^{0.5h} \frac{1}{k(Y)} dY \tag{3}$$

In hygro-thermal effect, the moisture rising is assumed to nonlinear distribution as a sinusoidal law (Nguyen *et al.* (2017))

$$C(Y) = (C_T - C_B) \left[ 1 - \cos \frac{\pi}{2} \left( \frac{2Y + h}{2h} \right) \right] + C_B \tag{4}$$

The kinematic equations are based on nonlinear relations because post-buckling phenomena is a geometrically nonlinear problem. In the nonlinear kinematic model, total Lagrangian approximation is used within the 2-D solid continuum model by using finite element method. Constitutive formulation with Green-Lagrange strain and second Piola-Kirchhoff stress with hygro-thermal effect is given as

$${}^1_0\mathbf{S} = \begin{Bmatrix} {}^1_0\mathbf{S}_{11} \\ {}^1_0\mathbf{S}_{22} \\ {}^1_0\mathbf{S}_{12} \end{Bmatrix} = \begin{bmatrix} {}_0\mathbf{C}_{11} & {}_0\mathbf{C}_{12} & 0 \\ {}_0\mathbf{C}_{12} & {}_0\mathbf{C}_{22} & 0 \\ 0 & 0 & {}_0\mathbf{C}_{66} \end{bmatrix} \begin{Bmatrix} {}^1_0\mathbf{E}_{11} - \alpha(Y)\Delta T - \beta(Y)\Delta C \\ {}^1_0\mathbf{E}_{22} \\ 2 {}^1_0\mathbf{E}_{12} \end{Bmatrix} \quad (5)$$

where  ${}^1_0\mathbf{S}_{11}$ ,  ${}^1_0\mathbf{S}_{22}$ ,  ${}^1_0\mathbf{S}_{12}$  are second Piola-Kirchhoff stress components,  ${}^1_0\mathbf{E}_{ij}$  is the Green-Lagrange strain components,  ${}_0\mathbf{C}_{ij}$  are the reduced constitutive tensor components,  $\alpha$  and  $\beta$  are thermal expansion and moisture expansion coefficients, respectively. Reduced constitutive tensor components are given as

$${}_0\mathbf{C}_{11} = {}_0\mathbf{C}_{22} = \frac{E(Y)}{1-\nu^2(Y)}, \quad {}_0\mathbf{C}_{12} = {}_0\mathbf{C}_{21} = \frac{\nu(Y)E(Y)}{1-\nu^2(Y)}, \quad {}_0\mathbf{C}_{66} = \frac{E(Y)}{2(1+\nu(Y))} \quad (6)$$

where  $E$  and  $\nu$  indicate the Young's modulus and Poisson's ratio, respectively. The Green-Lagrange strain components are stated in as follows

$${}^1_0\mathbf{E} = \begin{Bmatrix} {}^1_0\mathbf{E}_{11} \\ {}^1_0\mathbf{E}_{22} \\ 2 {}^1_0\mathbf{E}_{12} \end{Bmatrix} = \begin{Bmatrix} \frac{\partial u}{\partial X} + \frac{1}{2} \left[ \left( \frac{\partial u}{\partial X} \right)^2 + \left( \frac{\partial v}{\partial X} \right)^2 \right] \\ \frac{\partial v}{\partial Y} + \frac{1}{2} \left[ \left( \frac{\partial u}{\partial Y} \right)^2 + \left( \frac{\partial v}{\partial Y} \right)^2 \right] \\ \frac{\partial u}{\partial Y} + \frac{\partial v}{\partial X} + \frac{1}{2} \left[ \frac{\partial u}{\partial X} \frac{\partial u}{\partial Y} + \frac{\partial v}{\partial X} \frac{\partial v}{\partial Y} \right] \end{Bmatrix} \quad (7)$$

where  $u$  and  $v$  indicate displacement components in  $X$  and  $Y$  directions, respectively. Eight-node element plane element is considered in the finite element model (Figs. 2,3).

Total displacement ( $\delta$ ) and incremental displacement ( $\bar{\delta}$ ) fields are presented following equations

$$\{\delta\} = \begin{Bmatrix} u \\ v \end{Bmatrix} = \begin{Bmatrix} \sum_{j=1}^8 u_j \psi_j(x) \\ \sum_{j=1}^8 v_j \psi_j(x) \end{Bmatrix} \quad (8)$$

$$\{\bar{\delta}\} = \begin{Bmatrix} \bar{u} \\ \bar{v} \end{Bmatrix} = \begin{Bmatrix} \sum_{j=1}^8 \bar{u}_j \psi_j(x) \\ \sum_{j=1}^8 \bar{v}_j \psi_j(x) \end{Bmatrix} \quad (9)$$

where  $\psi$  is the shape functions. The shape functions for an eight-node element are as follows

$$\begin{aligned} [\psi_1] &= \left( X_e - \frac{L_x}{2} \right) \left( Y_e - \frac{L_y}{2} \right) \left( -\frac{1}{L_x L_y} - \frac{2X_e}{L_x^2 L_y} - \frac{2Y_e}{L_x L_y^2} \right) \\ [\psi_2] &= \left( \frac{4}{L_x L_y^2} \right) \left( X_e - \frac{L_x}{2} \right) \left( Y_e + \frac{L_y}{2} \right) \left( Y_e - \frac{L_y}{2} \right) \\ [\psi_3] &= \left( X_e - \frac{L_x}{2} \right) \left( Y_e + \frac{L_y}{2} \right) \left( \frac{1}{L_x L_y} + \frac{2X_e}{L_x^2 L_y} - \frac{2Y_e}{L_x L_y^2} \right) \\ [\psi_4] &= \left( \frac{4}{L_y L_x^2} \right) \left( X_e - \frac{L_x}{2} \right) \left( X_e + \frac{L_x}{2} \right) \left( Y_e - \frac{L_y}{2} \right) \end{aligned} \quad (10)$$

$$\begin{aligned}
 [\psi_5] &= \left(\frac{4}{L_y L_x^2}\right) \left(X_e - \frac{L_x}{2}\right) \left(X_e + \frac{L_x}{2}\right) \left(Y_e + \frac{L_y}{2}\right) \\
 [\psi_6] &= \left(X_e + \frac{L_x}{2}\right) \left(Y_e - \frac{L_y}{2}\right) \left(\frac{1}{L_x L_y} - \frac{2X_e}{L_x^2 L_y} + \frac{2Y_e}{L_x L_y^2}\right) \\
 [\psi_7] &= \left(-\frac{4}{L_x L_y^2}\right) \left(X_e + \frac{L_x}{2}\right) \left(Y_e + \frac{L_y}{2}\right) \left(Y_e - \frac{L_y}{2}\right) \\
 [\psi_8] &= \left(X_e + \frac{L_x}{2}\right) \left(Y_e + \frac{L_y}{2}\right) \left(-\frac{1}{L_x L_y} + \frac{2X_e}{L_x^2 L_y} + \frac{2Y_e}{L_x L_y^2}\right)
 \end{aligned}
 \tag{10}$$

In the  $i$  th iteration, the finite element equation is given as follows

$$\begin{bmatrix} K^{11L} + K^{11NL} & K^{12L} \\ K^{21L} & K^{22L} + K^{22NL} \end{bmatrix}^i \begin{Bmatrix} \bar{u} \\ \bar{v} \end{Bmatrix}^i = \begin{Bmatrix} -F^1 \\ -F^2 \end{Bmatrix}^i
 \tag{11}$$

where expressions of  $K$  indicate the tangent stiffness matrix, the expressions of  $F$  indicate the load vector at the  $i$  th iteration and  $p+1$ th load increment. The expressions of  $K$  and  $F$  are given in below

$$\begin{aligned}
 K_{ij}^{11L} &= b \int_A \left\{ {}_0C_{11} \left(1 + \frac{\partial u}{\partial X}\right)^2 \frac{\partial \psi_i}{\partial X} \frac{\partial \psi_j}{\partial X} + {}_0C_{22} \left(\frac{\partial u}{\partial Y}\right)^2 \frac{\partial \psi_i}{\partial Y} \frac{\partial \psi_j}{\partial Y} + \right. \\
 &\quad \left. {}_0C_{12} \left(1 + \frac{\partial u}{\partial X}\right) \left(\frac{\partial \psi_i}{\partial X} \frac{\partial \psi_j}{\partial X} + \frac{\partial \psi_i}{\partial Y} \frac{\partial \psi_j}{\partial X}\right) + {}_0C_{66} \left[\left(1 + \frac{\partial u}{\partial X}\right) \frac{\partial \psi_i}{\partial Y} + \frac{\partial u}{\partial Y} \frac{\partial \psi_j}{\partial X}\right] \times \left[\left(1 + \frac{\partial u}{\partial X}\right) \frac{\partial \psi_j}{\partial Y} + \frac{\partial u}{\partial Y} \frac{\partial \psi_i}{\partial X}\right] \right\} dXdY
 \end{aligned}
 \tag{12a}$$

$$\begin{aligned}
 K_{ij}^{11L} &= b \int_A \left\{ {}_0C_{11} \left(1 + \frac{\partial u}{\partial X}\right)^2 \frac{\partial \psi_i}{\partial X} \frac{\partial \psi_j}{\partial X} + {}_0C_{22} \left(\frac{\partial u}{\partial Y}\right)^2 \frac{\partial \psi_i}{\partial Y} \frac{\partial \psi_j}{\partial Y} + \right. \\
 &\quad \left. {}_0C_{12} \left(1 + \frac{\partial u}{\partial X}\right) \left(\frac{\partial \psi_i}{\partial X} \frac{\partial \psi_j}{\partial X} + \frac{\partial \psi_i}{\partial Y} \frac{\partial \psi_j}{\partial X}\right) + {}_0C_{66} \left[\left(1 + \frac{\partial u}{\partial X}\right) \frac{\partial \psi_i}{\partial Y} + \frac{\partial u}{\partial Y} \frac{\partial \psi_j}{\partial X}\right] \times \left[\left(1 + \frac{\partial u}{\partial X}\right) \frac{\partial \psi_j}{\partial Y} + \frac{\partial u}{\partial Y} \frac{\partial \psi_i}{\partial X}\right] \right\} dXdY
 \end{aligned}
 \tag{12b}$$

$$\begin{aligned}
 K_{ij}^{22L} &= b \int_A \left\{ {}_0C_{11} \left(\frac{\partial v}{\partial X}\right)^2 \frac{\partial \psi_i}{\partial X} \frac{\partial \psi_j}{\partial X} + {}_0C_{22} \left(1 + \frac{\partial v}{\partial Y}\right)^2 \frac{\partial \psi_i}{\partial Y} \frac{\partial \psi_j}{\partial Y} + \right. \\
 &\quad \left. {}_0C_{12} \left(1 + \frac{\partial v}{\partial Y}\right) \frac{\partial v}{\partial X} \left(\frac{\partial \psi_i}{\partial X} \frac{\partial \psi_j}{\partial X} + \frac{\partial \psi_i}{\partial Y} \frac{\partial \psi_j}{\partial X}\right) + {}_0C_{66} \left[\left(1 + \frac{\partial v}{\partial Y}\right) \frac{\partial \psi_i}{\partial X} + \frac{\partial v}{\partial X} \frac{\partial \psi_j}{\partial Y}\right] \times \left[\left(1 + \frac{\partial v}{\partial Y}\right) \frac{\partial \psi_j}{\partial X} + \frac{\partial v}{\partial X} \frac{\partial \psi_i}{\partial Y}\right] \right\} dXdY
 \end{aligned}
 \tag{12c}$$

$$K_{ij}^{11NL} = K_{ij}^{22NL} = b \int_A \left\{ {}_1S_{11} \frac{\partial \psi_i}{\partial X} \frac{\partial \psi_j}{\partial X} + {}_1S_{12} \left(\frac{\partial \psi_i}{\partial Y} \frac{\partial \psi_j}{\partial X} + \frac{\partial \psi_i}{\partial X} \frac{\partial \psi_j}{\partial Y}\right) + {}_1S_{22} \frac{\partial \psi_i}{\partial Y} \frac{\partial \psi_j}{\partial Y} \right\} dXdY
 \tag{12d}$$

$$\begin{aligned}
 F^1 &= b \int_A \left\{ {}_1S_{11} \left(1 + \frac{\partial u}{\partial X}\right) \frac{\partial \psi_i}{\partial X} + {}_1S_{22} \frac{\partial u}{\partial Y} \frac{\partial \psi_i}{\partial Y} + \right. \\
 &\quad \left. {}_1S_{12} \left[\left(1 + \frac{\partial u}{\partial X}\right) \frac{\partial \psi_i}{\partial Y} + \frac{\partial u}{\partial Y} \frac{\partial \psi_i}{\partial X}\right] \right\} dXdY
 \end{aligned}
 \tag{12e}$$

$$\begin{aligned}
 F^2 &= b \int_A \left\{ {}_1S_{11} \frac{\partial v}{\partial X} \frac{\partial \psi_i}{\partial X} + {}_1S_{22} \left(1 + \frac{\partial v}{\partial Y}\right) \frac{\partial \psi_i}{\partial Y} + \right. \\
 &\quad \left. {}_1S_{12} \left[\left(1 + \frac{\partial v}{\partial Y}\right) \frac{\partial \psi_i}{\partial X} + \frac{\partial v}{\partial X} \frac{\partial \psi_i}{\partial Y}\right] \right\} dXdY
 \end{aligned}
 \tag{12f}$$

In the solution of the nonlinear finite element of total Lagrangian formulations, small-step incremental method are used within Newton-Raphson iteration method. In the iteration steps, the

temperature rising is divided by large number. In Newton-Raphson method, the solution equation of problem in  $n+1$ th load increment and  $i$  th iteration is expressed as follows

$$d\delta_n^i = (\mathbf{K}_T^i)^{-1} \mathbf{R}_{n+1}^i \quad (13)$$

where  $\mathbf{K}_T^i$  is tangent stiffness matrix,  $d\delta_n^i$  is incremental displacement vector  $\mathbf{R}_{n+1}^i$  is residual vector and  $n+1$  is load increment in  $i$  th iteration. Iteration tolerance criterion is selected Euclidean norm as follows

$$\sqrt{\frac{[(d\delta_n^{i+1}-d\delta_n^i)^T (d\delta_n^{i+1}-d\delta_n^i)]^2}{[(d\delta_n^{i+1})^T (d\delta_n^{i+1})]^2}} \leq \zeta_{tol} \quad (14)$$

where

$$\delta_{n+1}^{i+1} = \delta_{n+1}^i + d\delta_{n+1}^i = \delta_n + \Delta\delta_n^i \quad (15)$$

$$\Delta\delta_n^i = \sum_{k=1}^i d\delta_n^k \quad (16)$$

The dimensionless quantities can be expressed as

$$T_R = \frac{\Delta T_T}{\Delta T_B}, \lambda = \delta^2 \alpha_B \Delta T_B, \delta = L/h, \bar{v} = v/L, \bar{X} = X/L, \bar{Y} = Y/L \quad (17)$$

where  $T_R$  indicates temperature ratio of top and bottom surfaces,  $C_R$  indicates moisture ratio of top and bottom surfaces,  $\lambda$  is the dimensionless temperature rising,  $\delta$  is the ratio of length and height,  $\bar{v}$  is the dimensionless vertical displacement,  $\bar{X}$  and  $\bar{Y}$  are dimensionless coordinates in the X and Y directions, respectively. If  $T_R = 1$ , temperature rising becomes uniform distribution, otherwise it becomes non-uniform distribution.

### 3. Numerical results

In this section, hygro-thermal post-buckling deflections, post-buckling configurations and critical buckling temperatures of the pinned-pinned FGM beam are calculated for different material distribution parameter, geometry parameters, temperature rising values and moisture rising values. The FGM beam is established by of Aluminum Oxide ( $E=349$  GPa,  $\nu=0.26$ ,  $\alpha = 6.86 \times 10^{-6}$ ,  $k=0.26$ ,  $\beta = 0.01$  wt %<sup>-1</sup>) at the bottom surface and Stainless Steel ( $E=201$  GPa,  $\nu=0.3262$ ,  $\alpha = 12.30 \times 10^{-6}$ ,  $k=15.37$ ,  $\beta=0.005$  wt %<sup>-1</sup>) at the top surface (Reddy (1998), Sobhy (2016)). In numerical study, the initial temperature value is selected as  $T_0=27$  °C. The geometry values of the beam are selected as:  $b = 0.2$  m,  $h = 0.2$  m and the length  $L$  is varied according to the  $\delta$  ratio in the numerical results. In the obtaining of the numerical results and graphs, the MATLAB program is used. It is noted that the moisture content of the bottom surface is changed and moisture content of the top surface  $C_T$  is constant  $C_T = 0 = \%0$  w in the numerical calculations. So, the hygro-thermal rising only rises at the bottom surface of FGM beam.

In order to verify the present formulation, special results of a similar work Nguyen *et al.* (2017) are compared with results of this study. In the comparison study, Normalized critical buckling temperatures of pinned-pinned FGM beam are obtained and compared with data presented in table 1 and table 4 of Nguyen *et al.* (2017) for different power-law parameter  $n$  for  $L/h=20$  for

Table 1 Comparison study: Normalized critical buckling temperatures of pinned-pinned FGM beam for different power-law parameter  $n$

	Dimensionless critical buckling temperatures					
	$n=0$	$n=0.5$	$n=1$	$n=2$	$n=5$	$n=10$
Nguyen <i>et al.</i> (2017)	1.309	0.970	0.878	0.812	0.752	0.714
Present	1.314	0.9716	0.884	0.823	0.768	0.724

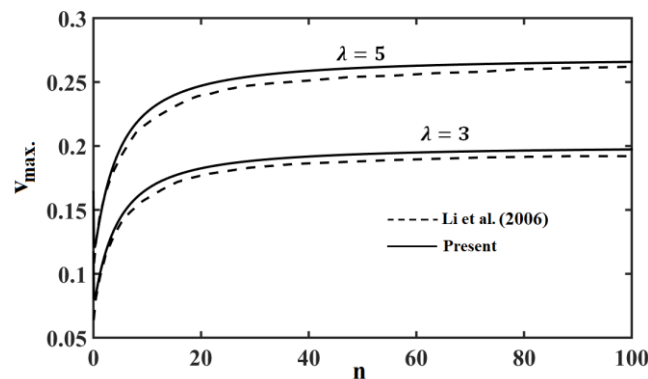
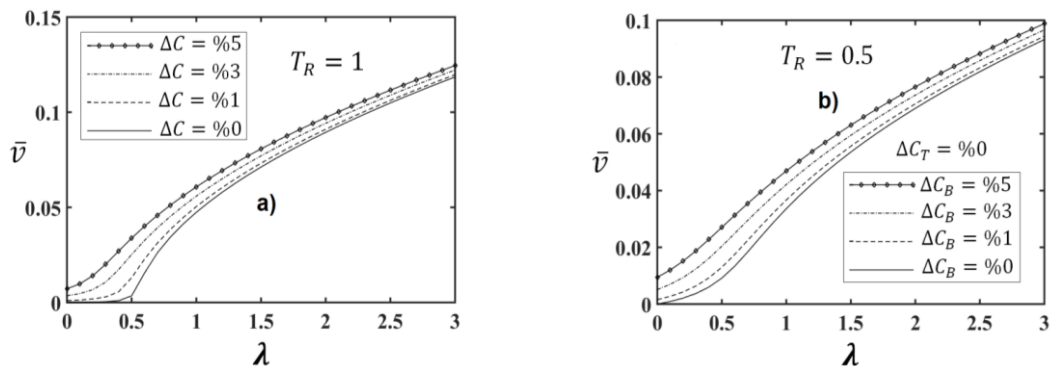


Fig. 4 Comparison study: The dimensionless maximum displacement versus  $n$  parameter for different dimensionless temperature rising



(a) for uniform hygro-temperature rising (b) for non-uniform hygro-temperature rising

Fig 5. Dimensionless temperature rising- dimensionless post-buckling vertical displacements curves for different moisture content values

temperature-independent case. The comparison study shows in Table 1 that the results of present study are very close to those of Nguyen *et al.* (2017).

To further compare this study, dimensionless max. post-buckling deflections of FGM beam for different values of  $T_R$ ,  $n$  and  $\lambda$  are obtained and compared with Li *et al.* (2006) for clamped-clamped beam and  $\delta = 15$  in figure 4. It is seen from figure 4 that the results of present study are very close to those of Li *et al.* (2006).

In Figs. 5(a) and 5(b), the effect of the moisture content on the maximum hygro-thermal post-buckling vertical deflections ( $v_{max}$ ) of the FGM beam are presented for  $n=0.5$ ,  $\delta = 10$  with

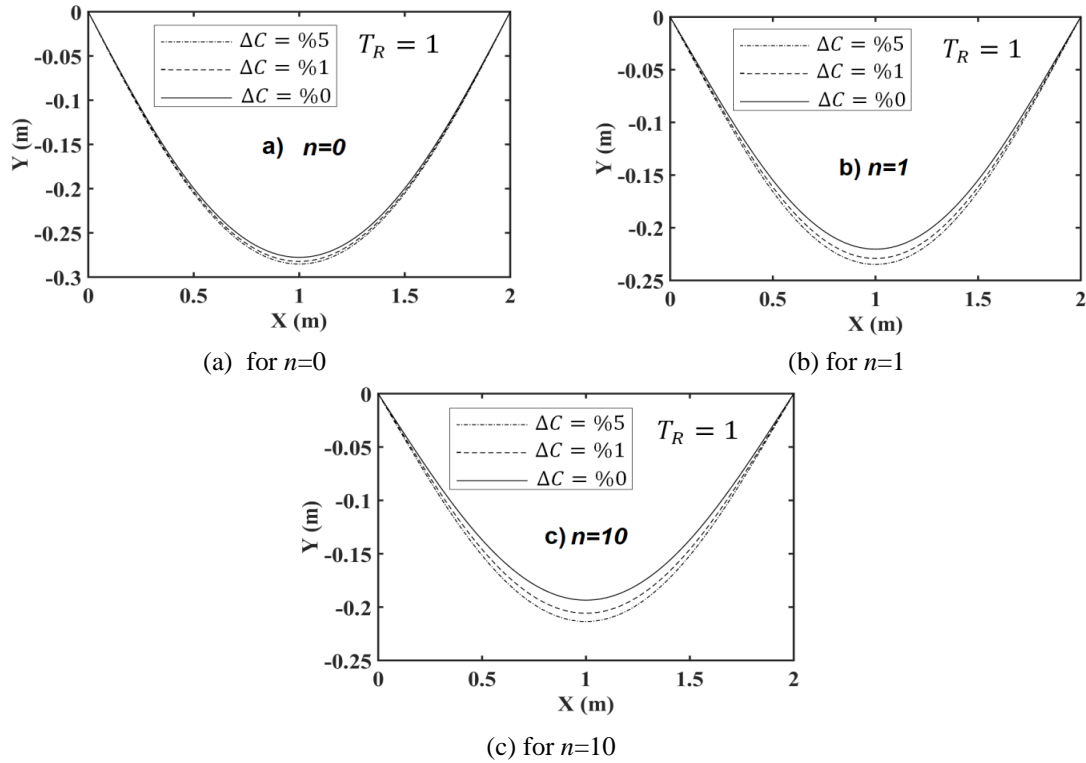


Fig. 6 The relationship between of the moisture content values and  $n$  in the hygro-thermal post-buckling deflected shape under uniform hygro-temperature rising

uniform and the non-uniform hygro-temperature rising, respectively. Also, the effects of the moisture content and material distribution (power-law parameter)  $n$  on the hygro-thermal post-buckling deflection shapes of the FGM beam are presented in figures 6 and 7. In figures 6 and 7, the hygro-thermal post-buckling deflected shapes are presented for  $\delta = 10$ ,  $\lambda = 3$  for under uniform and non-uniform hygro-temperature rising, respectively.

It is seen from Figs. 5 that increasing moisture content, post-buckling displacements increase significantly. Post-buckling deflections of FGM beams significantly change with moisture content rising. The post-buckling displacements converge significantly with increasing the temperature. Also, as seen from figure 5 that furcation points which gives the critical buckling temperatures decrease with moisture content rising. In higher values of moisture content, the buckling occurs even if the temperature rising do not occur ( $\lambda = 0$ ). In spite of the low values of temperatures, the buckling or post-buckling cases can occur with the moisture effects. The effect of moisture contents can be clearly seen in figures 6 and 7. Figures 6 and 7 show that although the values of temperature ( $\lambda = 3$ ) is stable, hygro-thermal post-buckling displacement configuration of FGM beam change considerably with increasing the moisture content. It shows that the moisture has important role on post-buckling behavior of FGM beams.

Fig. 8 highlights effects of moisture content on the relationship between the length/height ratio ( $\delta$ )-dimensionless critical buckling temperatures ( $\lambda_{cr}$ ) for  $n=0$  and  $T_R = 1$ . As seen in Fig. 8, increasing the moisture content yields to decreasing the critical buckling temperatures

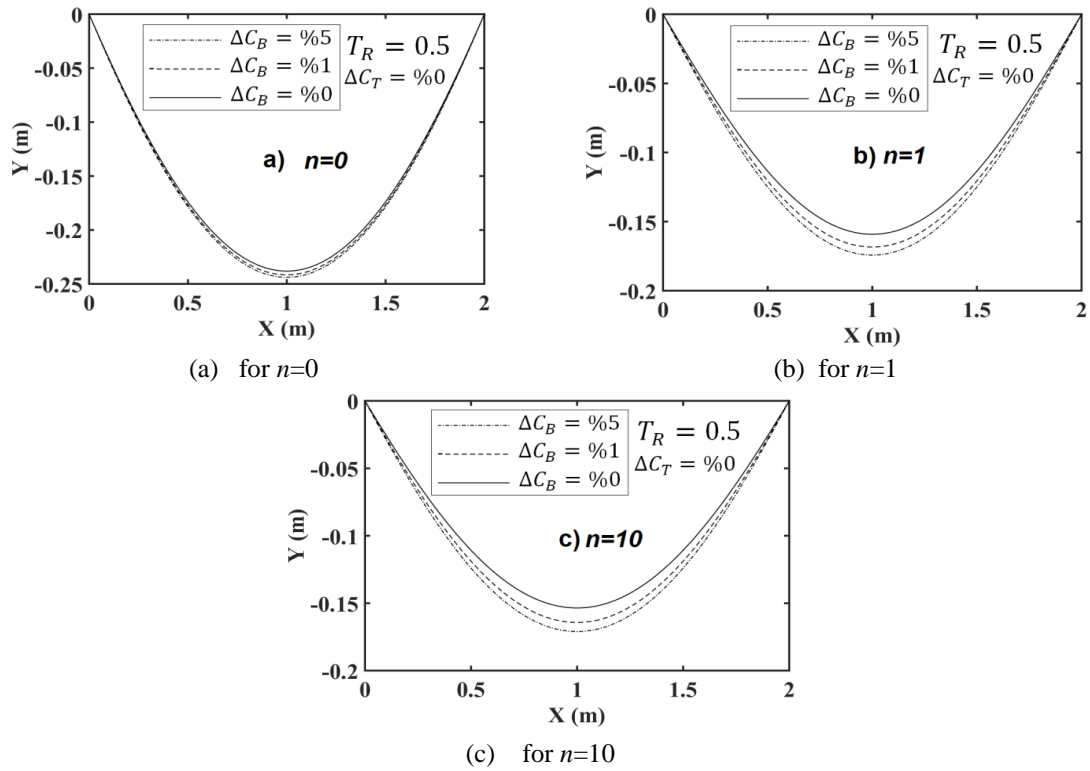


Fig. 7 The relationship between of the moisture content values and  $n$  in the hygro-thermal post-buckling deflected shape under non-uniform hygro-temperature rising

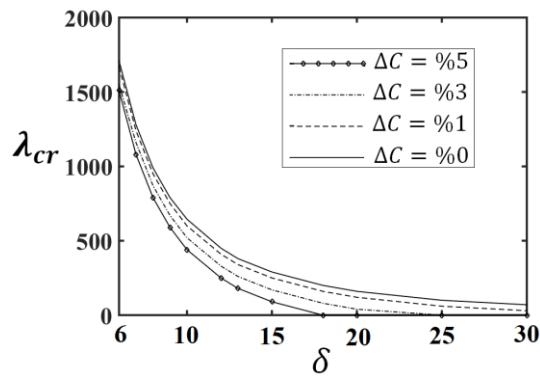


Fig. 8 Dimensionless critical temperature rising versus the ratio  $\delta = L/h$  for different the moisture content values

considerably. Also, the difference among moisture contents increases with increasing Lenth/height ratio. In higher values of  $\delta$ , the moisture is more effective in the critical buckling temperatures.

In Figs. 9(a) and 9(b) show effects of material distribution on dimensionless hygro-thermal post-buckling displacements with different moisture contents for  $\lambda = 3$ ,  $\delta = 10$  with uniform and the non-uniform hygro-temperature rising, respectively. As seen in Fig. 9, increasing  $n$  causes

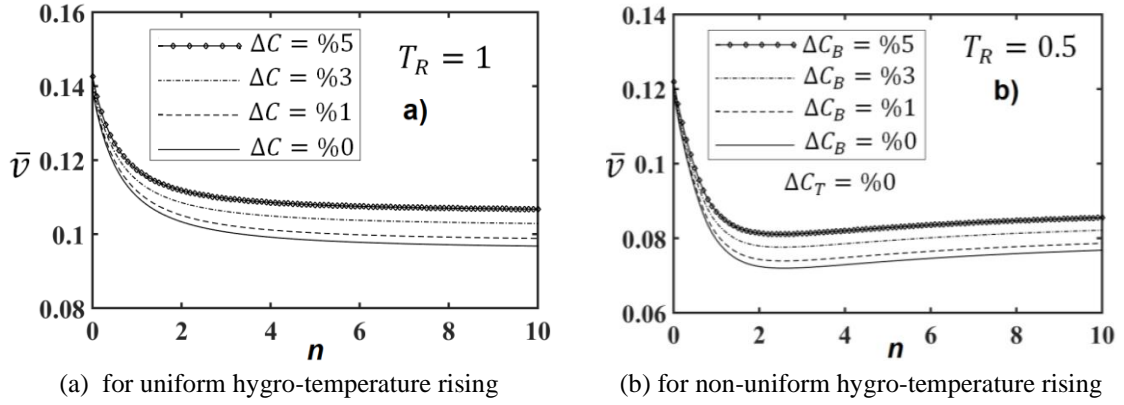


Fig. 9 The relationship between of the moisture content values and the power-law parameter  $n$  in the post-buckling displacements

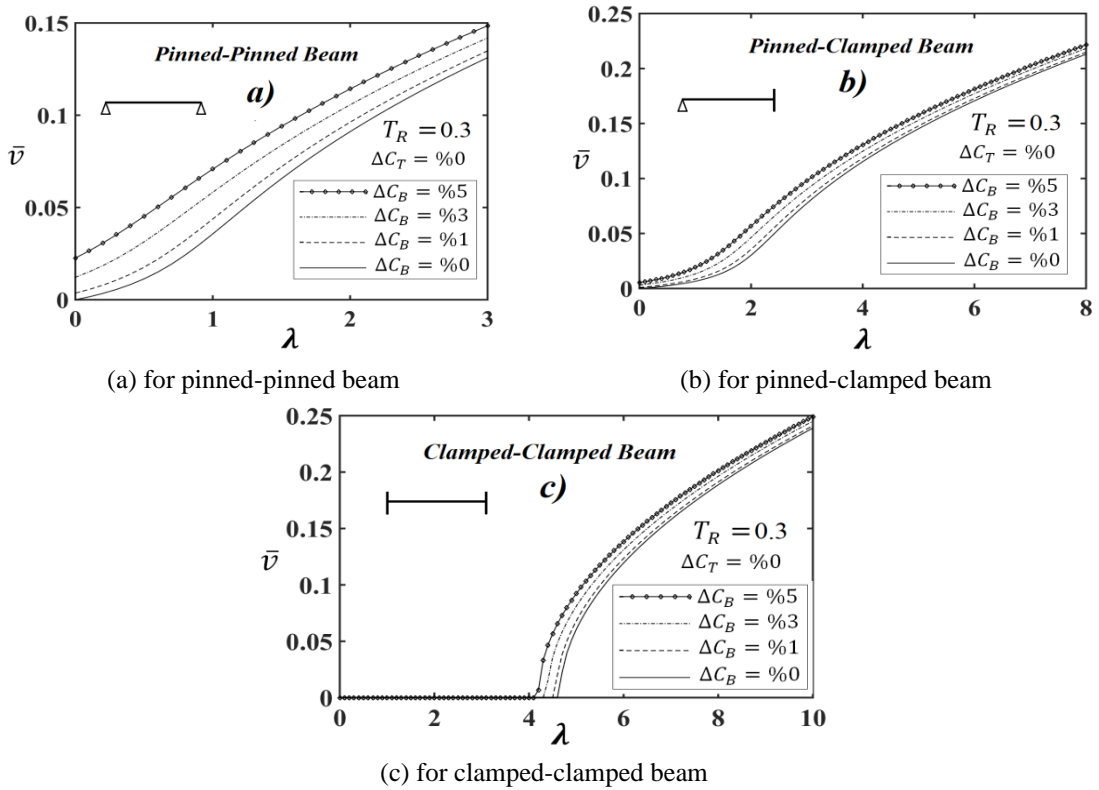


Fig. 10 The relationship between of the moisture content values and  $n$  in the hygro-thermal post-buckling deflected shape under non-uniform hygro-temperature rising

decreasing post-buckling displacements. The difference between among the moisture content values increases with increasing material distribution parameter. It shows that the material distribution parameter is very effective in hygro-thermal post-buckling responses of FGM beams. The effect of  $n$  can be clearly seen in Figs. 6 and 7. It is observed from Figs. 6 and 7 that  $n$

parameter play important role post-buckling deflections of FGM beam. Increase in  $n$ , nonlinear deflections of the FG beam decrease considerably. With increase in  $n$ , the beam material gets to homogeneous Aluminum Oxide (bottom surface material). The Young modulus of the Aluminum Oxide is bigger than Stainless Steel's. Hence, increasing the  $n$  yields to increase the elasticity modulus and rigidity of the beam increase.

In order to investigate the effects of different boundary conditions on the hygro-thermal post-buckling responses of FGM beam, the maximum hygro-thermal post-buckling vertical deflections ( $v_{max}$ ) are presented for  $n=1$ ,  $\delta = 10$ ,  $T_R = 0.3$  for pinned-pinned, pinned-clamped and clamped-clamped boundary conditions in Fig. 10.

It is seen from Fig. 10 that hygro-thermal effects in pinned-pinned beam is more bigger than the other boundary conditions. In clamped-clamped boundary condition, the moisture is less effective in the post-buckling responses. With increasing the moisture content, the post-buckling results less increase in contrast with other boundary conditions. It shows that the boundary conditions have important role on the hygro-thermal post-buckling responses of the FGM beams.

#### 4. Conclusions

Hygro-thermal post-buckling analysis of a FGM beam is investigated by finite element method within Total Lagrangian 2D continua and the Newton-Raphson iteration. The Effects of material distribution, geometry parameters, temperature rising and moisture changes on post-buckling responses of FGM beam are examined. The results showed that:

- The moisture plays important role on the post-buckling behavior of FGM beams.
- Increasing the moisture content yields to increasing post-buckling displacements and decreasing the critical buckling temperatures considerably.
- With increasing Length/height ratio, the effects of moisture on buckling/post-buckling behavior increase and the difference among moisture contents increases significantly.
- The material distribution parameter and boundary conditions of the beam are very effective in hygro-thermal post-buckling behavior of FGM beams.
- With increasing material distribution parameter, the difference among moisture contents increases.
- The superiority of two dimensional solid continua model to the other beam theories is that in the two dimensional solid continua model, more realistic results can be obtain without any assumptions.

#### References

- Abazid, M.A., Alotebi, M.S. and Sobhy, M. (2018), "A novel shear and normal deformation theory for hygrothermal bending response of FGM sandwich plates on Pasternak elastic foundation", *Struct. Eng. Mech.*, **67**(3), 219-232. <https://doi.org/10.12989/sem.2018.67.3.219>.
- Akbarzadeh, A.H. and Chen, Z.T. (2013), "Hygrothermal stresses in one-dimensional functionally graded piezoelectric media in constant magnetic field", *Compos. Struct.*, **97**, 317-331. <https://doi.org/10.1016/j.compstruct.2012.09.058>.
- Akbaş, Ş.D. (2014), "Large post-buckling behavior of Timoshenko beams under axial compression loads", *Struct. Eng. Mech.*, **51**(6), 955-971. <https://doi.org/10.12989/sem.2014.51.6.955>.
- Akbaş, Ş.D. (2015), "Wave propagation of a functionally graded beam in thermal environments", *Steel*

- Compos. Struct.*, **19**(6), 1421-1447. <http://dx.doi.org/10.12989/scs.2015.19.6.1421>.
- Akbaş, Ş.D. (2017a), "Nonlinear static analysis of functionally graded porous beams under thermal effect", *Coupled Syst. Mech.*, **6**(4), 399-415. <https://doi.org/10.12989/csm.2017.6.4.399>.
- Akbaş, Ş.D. (2017b), "Thermal effects on the vibration of functionally graded deep beams with porosity", *Int. J. Appl. Mech.*, **9**(5), 1750076. <https://doi.org/10.1142/S1758825117500764>.
- Akbaş, Ş.D. (2018a), "Nonlinear thermal displacements of laminated composite beams", *Coupled Syst. Mech.*, **7**(6), 691-705. <https://doi.org/10.12989/csm.2018.7.6.691>.
- Akbaş, Ş.D. (2018b), "Forced vibration analysis of functionally graded porous deep beams", *Compos. Struct.*, **186**, 293-302. <https://doi.org/10.1016/j.compstruct.2017.12.013>.
- Akbaş, Ş.D. (2018c), "Post-buckling responses of a laminated composite beam", *Steel Compos. Struct.*, **26**(6), 733-743. <https://doi.org/10.12989/scs.2018.26.6.733>.
- Akbaş, Ş.D. (2019), "Hygro-thermal nonlinear analysis of a functionally graded beam", *J. Appl. Comput. Mech.*, **5**(2), 477-485. <https://dx.doi.org/10.22055/jacm.2018.26819.1360>.
- Akbaş, Ş.D. and Kocatürk, T. (2012), "Post-buckling analysis of Timoshenko beams with temperature-dependent physical properties under uniform thermal loading", *Struct. Eng. Mech.*, **44**(1), 109-125. <https://doi.org/10.12989/sem.2012.44.1.109>.
- Akbaş, Ş.D. and Kocatürk, T. (2013), "Post-buckling analysis of functionally graded three-dimensional beams under the influence of temperature", *J. Therm. Stress.*, **36**(12), 1233-1254. <https://doi.org/10.1080/01495739.2013.788397>.
- Barati, M.R. (2017), "Vibration analysis of FG nanoplates with nanovoids on viscoelastic substrate under hygro-thermo-mechanical loading using nonlocal strain gradient theory", *Struct. Eng. Mech.*, **64**(6), 683-693. <https://doi.org/10.12989/sem.2017.64.6.683>.
- Beldjelili, Y., Tounsi, A. and Mahmoud, S.R. (2016), "Hygro-thermo-mechanical bending of SFGM plates resting on variable elastic foundations using a four-variable trigonometric plate theory", *Smart Struct. Syst.*, **18**(4), 755-786. <https://doi.org/10.12989/sss.2016.18.4.755>.
- Ebrahimi, F. and Habibi, S. (2018), "Nonlinear eccentric low-velocity impact response of a polymer-carbon nanotube-fiber multiscale nanocomposite plate resting on elastic foundations in hygrothermal environments", *Mech. Adv. Mater. Struct.*, **25**(5), 425-438. <https://doi.org/10.1080/15376494.2017.1285453>.
- Jouneghani, F.Z., Dimitri, R. and Tornabene, F. (2018), "Structural response of porous FG nanobeams under hygro-thermo-mechanical loadings", *Compos. Part B Eng.*, **152**, 71-78. <https://doi.org/10.1016/j.compositesb.2018.06.023>.
- Kaci, A., Houari, M.S.A., Bousahla, A.A., Tounsi, A. and Mahmoud, S.R. (2018), "Post-buckling analysis of shear-deformable composite beams using a novel simple two-unknown beam theory", *Struct. Eng. Mech.*, **65**(5), 621-631. <https://doi.org/10.12989/sem.2018.65.5.621>.
- Karami, B., Janghorban, M., Shahsavari, D. and Tounsi, A. (2018), "A size-dependent quasi-3D model for wave dispersion analysis of FG nanoplates", *Steel Compos. Struct.*, **28**(1), 99-110. <https://doi.org/10.12989/scs.2018.28.1.099>.
- Kocatürk, T. and Akbaş, Ş.D. (2011), "Post-buckling analysis of Timoshenko beams with various boundary conditions under non-uniform thermal loading", *Struct. Eng. Mech.*, **40**(3), 347-371. <https://doi.org/10.12989/sem.2011.40.3.347>.
- Kocatürk, T. and Akbaş, Ş.D. (2012), "Post-buckling analysis of Timoshenko beams made of functionally graded material under thermal loading", *Struct. Eng. Mech.*, **41**(6), 775-789. <https://doi.org/10.12989/sem.2012.41.6.775>.
- Laoufi, I., Ameer, M., Zidi, M., Bedia, E.A.A. and Bousahla, A.A. (2016), "Mechanical and hygrothermal behaviour of functionally graded plates using a hyperbolic shear deformation theory", *Steel Compos. Struct.*, **20**(4), 889-911. <https://doi.org/10.12989/scs.2016.20.4.889>.
- Lee, C.Y. and Kim, J.H. (2013), "Hygrothermal postbuckling behavior of functionally graded plates", *Compos. Struct.*, **95**, 278-282. <https://doi.org/10.1016/j.compstruct.2012.07.010>.
- Li, S.R., Zhang, J.H. Zhao, Y.G. (2006), "Thermal post-buckling of functionally graded material Timoshenko beams", *Appl. Math. Mech.*, **26**(6), 803-810. <https://doi.org/10.1007/s10483-006-0611-y>.

- Mohammadimehr, M., Salemi, M. and Navi, B.R. (2016), "Bending, buckling, and free vibration analysis of MSGT microcomposite Reddy plate reinforced by FG-SWCNTs with temperature-dependent material properties under hydro-thermo-mechanical loadings using DQM", *Compos. Struct.*, **138**, 361-380. <https://doi.org/10.1016/j.compstruct.2015.11.055>.
- Mouffoki, A., Adda Bedia, E.A., Houari, M.S.A., Tounsi, A. and Mahmoud, S.R. (2017), "Vibration analysis of nonlocal advanced nanobeams in hygro-thermal environment using a new twounknown trigonometric shear deformation beam theory", *Smart Struct. Syst.*, **20**(3), 369-383. <https://doi.org/10.12989/sss.2017.20.3.369>.
- Nguyen, T.K., Nguyen, B.D., Vo, T.P. and Thai, H.T. (2017), "Hygro-thermal effects on vibration and thermal buckling behaviours of functionally graded beams", *Compos. Struct.*, **176**, 1050-1060. <https://doi.org/10.1016/j.compstruct.2017.06.036>.
- Radwan, A.F. (2019), "Effects of non-linear hygrothermal conditions on the buckling of FG sandwich plates resting on elastic foundations using a hyperbolic shear deformation theory", *J. Sandw. Struct. Mater.*, **21**(1), 289-319. <https://doi.org/10.1177%2F1099636217693557>.
- Reddy, J.N. and Chin, C.D. (1998), "Thermomechanical analysis of functionally graded cylinders and plates", *J. Therm. Stress.*, **21**(6) 593-626. <https://doi.org/10.1080/01495739808956165>.
- Sobhy, M. (2016), "An accurate shear deformation theory for vibration and buckling of FGM sandwich plates in hygrothermal environment", *Int. J. Mech. Sci.*, **110**, 62-77. <https://doi.org/10.1016/j.ijmecsci.2016.03.003>.
- Zenkour, A. (2013), "Hygrothermal analysis of exponentially graded rectangular plates", *J. Mech. Mater. Struct.*, **7**(7), 687-700. <http://dx.doi.org/10.2140/jomms.2012.7.687>.